Chapter 3. Improved Ordering in Low Molecular Weight Protein-Polymer Conjugates Through Oligomerization of the Protein Block

3.1 Abstract

The self-assembly of protein-polymer conjugates incorporating oligomers of a small, engineered high-affinity binding protein, rcSso7d.SA, is studied to determine the effect of protein oligomerization on nanoscale ordering. Oligomerization enables a systematic increase in the protein molar mass without changing its overall folded structure, leading to a higher driving force for self-assembly into well-ordered structures. Though conjugates of monomeric rcSso7d.SA are found to only exist in disordered states, oligomers of this protein linked to a poly(*N*-isopropylacrylamide) (PNIPAM) block self-assemble into lamellar nanostructures. Conjugates of trimeric and tetrameric rcSso7d.SA are observed to produce the strongest ordering in concentrated solution, displaying birefringent lamellae at concentrations as low as 40 wt. %. In highly concentrated solution, the oligomeric rcSso7d.SA-PNIPAM block copolymers exhibit ordering and domain spacing trends atypical from that of most block copolymers. Fluorescent binding assays indicate that oligomerized protein blocks retain binding functionality and exhibit limits of detection up to three times lower than that of surface-immobilized protein sensors. Therefore, oligomerization of the protein block in these block copolymers serves as an effective method to improve both nanoscale ordering and biosensing capabilities.

3.2 Introduction

The highly-specific molecular recognition capabilities of proteins have enabled their widespread use in a variety of biosensor formats including lateral flow assays,[1-4] microfluidics,[5-8] and

microarrays.[9-10] In each of these biosensors, proteins are immobilized on a surface, where device sensitivity is enhanced by achieving densely-packed proteins that are well-oriented to allow free access to binding sites.[11-13] The simplest and most general methods for protein surface functionalization involve covalent anchoring via free amines on the surfaces of proteins. Because these amines are distributed at multiple points across the protein surface, however, the resulting orientation is random, reducing the active proportion of the surface-immobilized binding protein. As such, there is significant interest in developing techniques that enable site-specific immobilization. Current directed immobilization strategies include modifying functional groups that appear at only a single location on a protein,[14-15] adding ssDNA fragment linkers,[16] or fusing to proteins[17-18] and installing tags[19-20] that display high binding affinity to a specific surface. While all of these methods can be used to orient proteins and improve biosensor performance, these approaches can only be used for specific classes of proteins or require significant protein and/or surface pre-treatment.

One potentially straightforward and effective technique for creating a dense array of properly oriented proteins is through utilization of block copolymer-like self-assembly. By conjugating a protein to a polymer and dissolving the bioconjugate in concentrated aqueous solution, it has been demonstrated that these conjugates assemble into ordered nanostructures similar to coil-coil diblock copolymers.[21-23] While the individual ordered phases in both types of diblock copolymers are identical, the self-assembly of protein-polymer conjugates exhibits notable differences from that of traditional block copolymers. Protein-polymer conjugates display highly asymmetric phase behavior[24] and re-entrant order-disorder transition (ODT) behavior,[24-25] in contrast to the enhanced ordering in more concentrated block copolymer solutions predicted by the dilution approximation.[26] A complete explanation for these deviations from characteristic

block copolymer assembly has not yet been established, but it is known that coarse-grained features of the conjugates have significant effects on self-assembly: polymer topology,[27] polymer chemistry,[25] protein shape,[28] and electrostatics[29] have all been found to significantly affect phase behavior and ordering in protein-polymer block copolymers.

Initial studies have been performed on the activity and binding capabilities of enzymatic coatings and sensors developed from these conjugates. Thin films of myoglobin-*b*-poly(*N*-isopropylacrylamide) (PNIPAM) formed weakly-ordered lamellae in solution and exhibited up to a 10-fold improvement in catalytic activity compared to common surface-immobilization techniques.[30] Similar antibody-PNIPAM thin film biosensors displayed a two order of magnitude decrease in the limit of detection compared to an antibody monolayer and a linear relationship between the number of binding events and film thickness, which is related to the total amount of protein in the film.[31] These studies suggest that the increased number of proteins that can be immobilized on a surface in 3D arrays achieved through protein-polymer diblock copolymer self-assembly can greatly enhance protein catalytic and sensing capabilities.

While protein-polymer conjugates incorporating antibodies as the protein block have been shown to function as highly sensitive biosensors, there is a growing trend toward using small proteins as affinity elements in sensors due to their enhanced stability and the ease with which they can be recombinantly expressed. For example, nanobodies—the 12-15 kDa single binding domain of heavy chain-only antibodies—have been incorporated into biosensors to achieve improved sensitivities compared to antibody-based sensors due to the greater surface functionalization achievable with these smaller proteins.[32] This sensitivity improvement is more clearly seen in electrochemical sensors[33-34] where the decreased distance between binding events and the surface has resulted in increased signal strength. Small engineered affinity binding proteins have also

received more frequent use as sensors within the past decade. A class of 6 kDa proteins consisting of a three-helix bundle, affibodies, have been demonstrated to function effectively in microarray formats.[35-36] Similarly, 7 kDa DNA-binding proteins, particularly Sac7d and Sso7d, have been designed to bind with antibody-level affinities to a variety of targets.[37-39] Though their use in biosensors has only recently been explored,[18, 39-40] these engineered DNA-binding protein mutants display exceptional stability over a wide pH and temperature range,[41] making them attractive candidates for sensors that remain functional in conditions under which proteins typically unfold.

There are numerous potential benefits to using small proteins in biosensors fabricated from protein-polymer conjugates, but the weak ordering in these conjugates containing a small protein block remains a barrier to maximizing device sensitivity by self-assembly. In traditional coil-coil block copolymers, ordered phases are only observed when the overall degree of polymerization of the diblock copolymer is large enough to sufficiently reduce the entropic penalty due to chain stretching that occurs at the interfaces between domains. While the self-assembly of protein-polymer block copolymers is not fully understood, similar trends have been observed in these materials. Model studies using the fluorescent protein mCherry as the protein block in these conjugates have found that no ordered structures are observed at low coil fractions ($0.2 \leq f \leq 0.3$),[24] and at intermediate coil fractions ($0.3 \leq f \leq 0.5$), structures are significantly weaker ordered than the corresponding phases at high coil fractions ($0.5 \leq f \leq 0.75$).[24-25] Thus, exploring approaches to increase the molecular weight of the protein block in protein-polymer conjugates may yield methods to create well-ordered structures of these conjugates incorporating a low molecular weight protein.

Herein, the effect of increasing molecular weight of low molecular weight protein blocks on ordering in protein-polymer conjugates is explored using protein blocks incorporating an Sso7d

mutant engineered to bind strongly to streptavidin, rcSso7d.SA.[39] Oligomers of rcSso7d.SA are created by linking the proteins with short, flexible peptide sequences, and the phase behavior of conjugates of these oligomers—monomer to tetramer—with PNIPAM is studied. While conjugates of monomeric rcSso7d.SA are disordered under all conditions studied, conjugates of oligomeric rcSso7d.SA are observed to self-assemble into well-ordered lamellar structures. The biosensing capabilities of these conjugates are also explored, and it is discovered that the trimer conjugates provide over a 3-fold reduction in limit of detection compared to monolayers of rcSso7d.SA.

3.3 Materials and Methods

3.3.1 Synthesis

Poly(*N*-isopropylacrylamide) (PNIPAM) functionalized with a maleimide group was synthesized by reversible addition-fragmentation chain transfer (RAFT) polymerization, as described previously.[21] Polymer molecular weight and dispersity were characterized by gel permeation chromatography performed on an Agilent 1260 LC system equipped with two columns (ResiPore, 300 × 7.5 mm, up to 500k Da, Agilent Technologies, CA) in series, a Wyatt miniDAWN TREOS multi-angle light scattering detector, and a Wyatt Optilab T-rEX diffractometer (**Figure B-1**). DMF with 0.02 LiBr was used as the mobile phase with a flow rate of 1 mL/min at 70 °C.

Details for the construction of genes for monomeric, dimeric, trimeric, and tetrameric rcSso7d.SA each containing an N-terminal Cys residue are provided in **Chapter 2**. Each gene was inserted into a pET28b(+) vector, which encodes an N-terminal 6xHis tag, and transformed into BL21(de3) *E.coli* cells. Each protein was expressed in 1 L of Terrific Broth at 37 °C inoculated with 5 mL of overnight culture and induced with 1 mM isopropyl-β-D-1-thiogalactopyranoside (IPTG) at an OD_{600} of 0.8-1.0. After induction the cells were cultured at 20 °C for 18-20 hours and

harvested. The cells were resuspended in lysis buffer (50 mM NaH_2PO_4, 300 mM NaCl, 10 mM imidazole, 10 mM β-mercaptoethanol (BME), pH 8.0) and frozen at -80 °C overnight. After thawing, the cells were lysed by ultrasonication. The lysate was clarified by centrifugation, and the protein was purified using Ni-NTA metal affinity chromatography. Throughout the purification, 10 mM BME was used in all buffers. Elution fractions containing purified protein were immediately exchanged into resuspension buffer (50 mM Tris buffer, 100 mM NaCl, 0.25 mM tris(2-carboxyethyl)phosphine (TCEP), pH 7.4) by performing a 1000x buffer exchange in Millipore-Ultra 15 centrifugal filters (molecular weight cutoff of 3 kDa for monomeric rcSSo7d.SA or 10 kDa for rcSso7d.SA oligomers). The purity of the protein was confirmed by denaturing gel electrophoresis (SDS-PAGE) (**Figure A-2a**). Protein concentration was determined by performing a reducing-agent compatible BCA assay, and proper secondary structure folding of the proteins was assessed using circular dichroism (CD) (**Figure A-3a**). The typical yields of purified protein for the monomeric, dimeric, trimeric, and tetrameric rcSso7d.SA species were 120, 160, 75, and 40 mg per liter of culture, respectively.

3.3.2 Bioconjugation and Preparation of Bulk Samples

Bioconjugations between rcSso7d.SA oligomers and maleimide-functionalized PNIPAM were performed in resuspension buffer. Solutions of rcSso7d.SA oligomers were diluted to approximately 5 mg/mL, and a 5x molar excess of PNIPAM was added. After complete dissolution of PNIPAM, samples were incubated at 4 °C for 24 h. Ammonium sulfate was then added to a concentration of 1.0 M to remove unconjugated protein. Following centrifugation, the supernatant was discarded and the precipitates were resuspended in resuspension buffer to approximately 5 mg/mL. Two additional ammonium sulfate precipitations were performed, after which the resulting solution was purified by Ni-NTA chromatography to remove unconjugated PNIPAM.

Purified protein-PNIPAM conjugates were dialyzed against MilliQ water. Bioconjugate purity was confirmed using SDS-PAGE and Native PAGE (**Figure A-2b-c**), and retention of protein secondary structure was assessed using CD (**Figure A-3b**). Conjugate solution was concentrated to approximately 100 mg/mL using Millipore-Ultra 15 centrifugal filters (molecular weight cutoff of 10 kDa). Bulk solid samples were prepared by drop-casting aliquots of this concentrated solution onto Teflon sheets and drying under vacuum to a final pressure of 5 Torr (ramp rate 50 Torr/h) at room temperature. Samples were then collected and stored at 4 °C until future use. Typical yields after purification ranged from 50% with monomeric rcSso7d.SA to 25% with tetrameric rcSso7d.SA.

3.3.3 Solution-phase Sample Preparation and Characterization

Dehydrated samples were rehydrated in MilliQ water at 4 °C to the desired concentration immediately prior to use. The concentrated solution phase behavior of rcSso7d.SA-PNIPAM conjugates was characterized using small-angle X-ray scattering (SAXS) (**Figures B-2 to B-5**), depolarized light scattering (DPLS) and turbidimetry (**Figures B-6 to B-9**), and differential scanning calorimetry (DSC) (**Figure B-10**). Details of the sample preparation and measurement conditions for these techniques are provided in **Chapter 2**.

3.3.4 Thin Film Preparation

Silicon wafers (Wafer World, P-type Silicon with boron as dopant, (100) orientation, single-side polished) were cut into 0.9 cm-by-5 cm sections and sequentially and thoroughly rinsed with acetone, methanol, and water. Wafers were then dried under a filtered air flow and treated with oxygen plasma for 3 minutes. Immediately following plasma cleaning, conjugate samples rehydrated to 10 wt.% in MilliQ water were flow coated onto the silicon wafers in a chamber maintained at 60% relative humidity, as described previously.[42] To stabilize thin films against

dissolution in water, the cast films were preheated to 40 °C and immersed in a 1.4 wt.% aqueous solution of glutaraldehyde at 40 °C for 20 s to lightly crosslink the protein nanodomains. Immediately following immersion, thin films were thoroughly rinsed with water until the surfaces became hydrophilic, indicating complete removal of unlinked glutaraldehyde. Films were dried under filtered airflow and stored at ambient conditions until use. Film thickness was determined using a Woolam M-2000D spectroscopic ellipsometer using a single incidence angle of 70°. Curves were fit using a three-layer model consisting of a 0.4 mm bottom silicon substrate, a native silicon oxide layer of 18 Å, and a top conjugate layer fit using a Cauchy model. rcSso7d.SA monolayers were prepared by coupling protein activated by 1-Ethyl-3-(3-dimethylaminopropyl)carbodiimide/N-hydroxysuccinimide (EDC/NHS) with amine-functionalized silicon wafers using literature methods.[43]

3.3.5 Fluorescence Assays

The binding function of rcSso7d.SA oligomer-PNIPAM thin films was measured using fluorescently-labeled monomeric streptavidin (mSA2). Details for the expression, purification, and fluorescent labeling of mSA2 are provided in **Chapter 2**. 0.5 µL drops of solutions containing serially diluted fluorescent mSA2 samples in PBS (pH 7.4) were gently applied to the surface of each bioconjugate thin film. Films were incubated in a sealed chamber saturated with water vapor at room temperature to prevent to prevent drying of the applied fluorescent samples. After 1 hour, films were thoroughly rinsed with water, dried under filtered airflow, and immediately analyzed for fluorescent signal. Fluorescence microscopy images were acquired at 4x magnification using a Cy5 filter set and exposure time of 5000 ms on an Olympus IX-81 inverted fluorescence microscope with an AxioCam HRC CCD camera. Fluorescent intensity was calculated using ImageJ software[44] by determining the average fluorescent signal in a rectangular area of the

fluorescent image free of defects and occupying no less than half of the full sample application area.

3.4 Results and Discussion

3.4.1 Phase Behavior

Oligomers of rcSso7d.SA, a modified DNA-binding protein designed to exhibit high-affinity streptavidin binding,[39] linked together by flexible $(Gly_4Ser)_2$ peptides (**Figure 3-1a**),[46] were expressed and conjugated to poly(*N*-isopropylacrylamide) (PNIPAM) (**Figure 3-1b**). Each oligomer—hereafter referred to as *n*x rcSSo7d.SA, where *n* is the number of rcSso7d.SA proteins in the oligomer—was conjugated to PNIPAM of comparable molar mass as the oligomer (**Table 3-1**). A PNIPAM volume fraction could not be calculated for these protein-polymer block copolymers since the molar volume of the protein is not known, so all conjugates were synthesized with symmetric weight fraction, as this is the approximate condition at which optimal ordering has previously been observed in protein-polymer conjugates.[24]

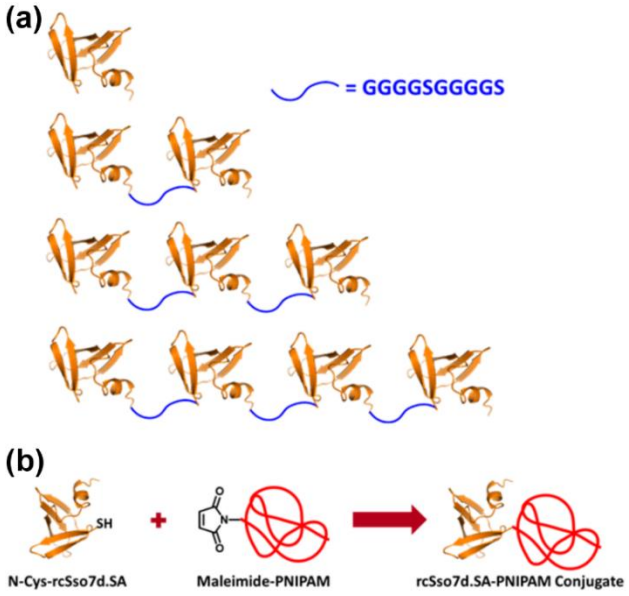

Figure 3-1. (a) Representation of rcSso7d.SA oligomers. From top to bottom: 1x rcSso7d.SA, 2x rcSso7d.SA, 3x rcSso7d.SA, 4x rcSso7d.SA. (b) General schematic of N-Cys-rcSso7d.SA oligomer conjugation to maleimide end-functionalized PNIPAM. Protein is a cartoon representation of the Sso7d crystal structure (PDB 1SSO).[45]

Table 3-1. Composition of rcSso7d.SA oligomer-PNIPAM Conjugates

Conjugate	Protein	Protein MW (kDa)	PNIPAM M_n (kDa)	PNIPAM Đ	PNIPAM Weight Fraction
1xSP9.8k	1x rcSso7d.SA	9.4	9.8	1.09	0.51
2xSP17k	2x rcSso7d.SA	17.1	16.8	1.10	0.50
3xSP25k	3x rcSso7d.SA	24.9	24.9	1.10	0.50
4xSP30k	4x rcSso7d.SA	32.5	30.0	1.10	0.48

Analysis of the four studied conjugates in concentrated solution suggests a clear effect of oligomerization (molar mass) on morphology. Phase diagrams are constructed for each conjugate (**Figure 3-2**) using SAXS to determine nanostructure periodicity, DPLS to assess long-range ordering, turbidimetry to determine transitions to macrophase separated states, and DSC to estimate PNIPAM desolvation temperatures (**Table 3-2**). While the conjugates are assumed to exhibit equilibrium morphology under most of the studied conditions, 100 wt. % samples created by drying solutions under vacuum at a controlled pressure ramp rate of 50 Torr/h are known to be kinetically trapped in a weakly-ordered morphology.[24]

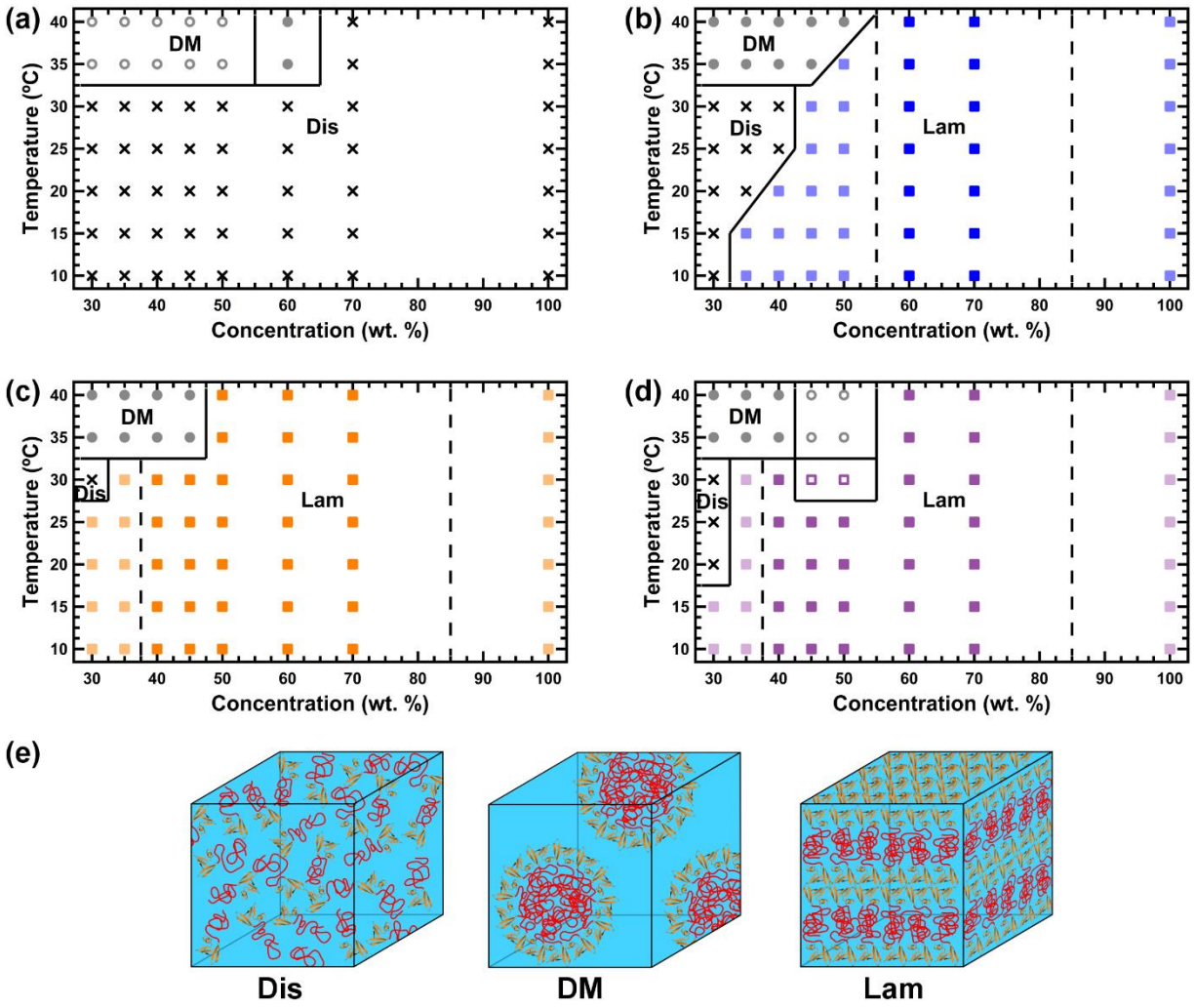

Figure 3-2. Phase diagrams of (a) 1xSP9.8k, (b) 2xSP17k, (c) 3xSP25k, and (d) 4xSP30k as a function of concentration and temperature. Phases are assigned in the diagrams as disordered (Dis), disordered micellar (DM), or lamellar (Lam) and are also (e) represented schematically. Light colored symbols represent non-birefringent lamellar phases, which are separated by dashed lines from shaded colored symbols representing birefringent lamellar phases. Solid symbols indicate a homogeneous phase, while open symbols indicate a macrophase-separated phase.

Table 3-2. Thermal Transitions for rcSso7d.SA Oligomer-PNIPAM Conjugates in Concentrated Solution

Conjugate	Conc. (wt. %)	T_{DPLS}[a] (°C)	T_t[b] (°C)	T_{DSC}[b] (°C)
1xSP9.8k	30	○	30.1	29.6
	35	○	30.3	29.0
	40	○	30.9	28.5
	45	○	34.2	27.2
	50	○	31.3	25.5
	60	●	--	24.8
	70	○	--	--
2xSP17k	30	○	--	28.7
	35	○	--	28.6
	40	○	--	27.3
	45	○	--	26.1
	50	○	--	25.4
	60	●	--	--
	70	●	--	--
3xSP25k	30	○	--	27.8
	35	○	--	28.4
	40	●	--	28.0
	45	●	--	26.6
	50	●	--	26.1
	60	●	--	23.0
	70	●	--	--
4xSP30k	30	○	--	29.4
	35	○	--	28.3
	40	●	--	27.5
	45	●	26.1	26.0
	50	●	26.7	25.4
	60	●	--	22.1
	70	●	--	--

[a]○ denotes samples that never display birefringent behavior within the studied temperature range. ● denotes samples that remain birefringent throughout the entire studied temperature range. [b]The symbol "--" signifies that no thermal transition is observed at the given concentration.

Conjugates containing oligomerized rcSso7d.SA protein blocks are observed to exhibit well-ordered structures. 1xSP9.8k remains disordered under all studied conditions (**Figure 3-2a**), but all oligomer conjugates display lamellar morphology over a wide concentration range (**Figures 3-2b-d**). The size of disordered regions in the phase diagrams also generally shrinks with increasing molecular weight of the protein block: 2xSP17k remains disordered up to concentrations of 40 wt. %, whereas 3xSP25k and 4xSP30k only display a disordered phase at 30

wt. %. Accordingly, the order-disorder transition concentration (C_{ODT}) is decreased for higher-order oligomer conjugates, with values of 45, 35, and ≤ 30 wt. % (only concentrations as low as 30 wt. % were studied) for 2xSP17k, 3xSP25k, and 4xSP30k, respectively. Concentration ranges over which birefringent lamellae can be seen follow a similar trend, as the range expands from 60-70 wt. % for 2xSP17k to 40-70 wt. % for 3xSP25k and 4xSP30k.

Despite the significant differences in ordering between the four oligomer conjugates, their phase diagrams contain many similar attributes. At high temperatures where water is selective for the protein block, PNIPAM blocks collapse inward away from a water-rich phase, resulting in the formation of disordered micelles. As can be seen in the SAXS curves (**Figure 3-3a**), increasing temperature results in a gradual decrease in intensity of the scattering peaks corresponding to periodic nanostructures, but above the PNIPAM transition temperature, these peaks are almost entirely replaced by form factor scattering from the micelles. In 1xSP9.8k and 4xSP30k solutions, macrophase separated regions between conjugate-rich and conjugate-poor phases of disordered micelles exist, and these regions always exist above the PNIPAM thermal transition temperature (**Table 3-2**). As concentration increases, the temperature at which this transition to a macrophase separated state occurs also increases, which has been attributed to the ability of the protein domains to accommodate water.[23] Once PNIPAM chains begin to collapse and expel water above their thermal transition temperature, the excess water is initially accommodated through swelling of the protein domains. Above a certain temperature, the excess water can no longer be taken up by the proteins, resulting in the separation of micelles from a water-rich phase. As conjugate concentration increases, more protein is present to accommodate water from collapsed PNIPAM chains, so the macrophase separation transition temperature increases and—at high

concentrations—does not occur below 40 °C, indicating that the water is fully accepted into the protein domains.

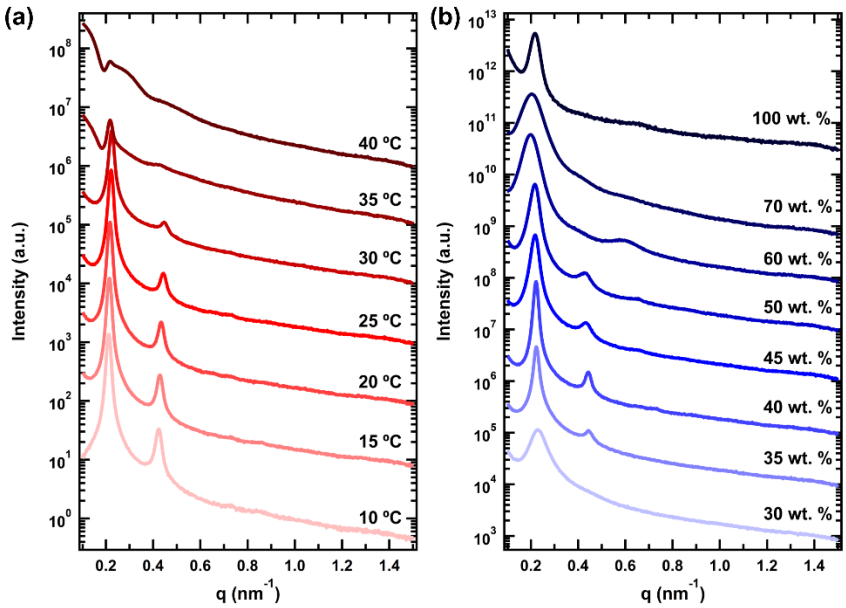

Figure 3-3. SAXS curve displaying changes in conjugate phase behavior with (a) temperature and (b) concentration. Both graphs contain data for 4xSP30k at either (a) 40 wt. % or (b) 25 °C and are representative of trends observed across all studied conjugates.

Many similarities also exist between the three conjugates that form ordered phases. Below the thermal transition temperature of PNIPAM where water acts as a good solvent for both blocks, lamellar phases are observed. This strong preference for lamellae is consistent with phase behavior in rod-coil diblock copolymers,[47] which, similar to protein-polymer block copolymers, contain one rigid and one flexible block. Unlike previous work analyzing the self-assembly of protein-PNIPAM conjugates of mCherry and GFP,[28] no hexagonally packed cylinder phase is observed in any of the rcSso7d.SA oligomer conjugates. However, this phase was only seen when PNIPAM represented the minority block in both volume and weight fraction. In this study where only symmetric diblocks were considered, it is likely that the volume fraction of the polymer block is not low enough to thermodynamically favor bending of the protein-polymer interface to form cylindrical nanodomains. Below 45 wt. %, increases in concentration promote the formation of

well-defined lamellar phases (**Figure 3-3b**) with increasing birefringence (**Figures B-6 to B-9**) for 2xSP17k, 3xSP25k, and 4xSP30k. In highly concentrated solutions, though, ordering worsens as peaks significantly broaden, which is suggestive of the re-entrant order-disorder transition (ODT) behavior that has been previously observed in protein-polymer conjugates.[24-25]

DSC measurements of PNIPAM desolvation temperatures reveal clear trends within and across the studied rcSso7d.SA oligomer-PNIPAM conjugates. All four conjugates display decreasing transition temperatures with increasing concentration, consistent with previous findings in protein-polymer conjugates.[23, 28-29] As the molecular weight of the PNIPAM block increases, the transition temperatures at a given concentration also generally decrease. This trend agrees with findings for homopolymer solutions of PNIPAM and other polymers with LCST behavior:[48] as polymer molecular weight increases, the exothermic contribution from polymer solvation decreases relative to the magnitude of the entropic penalty associated with the corresponding decrease in solvent free volume.[49] However, the PNIPAM desolvation temperature appears to be a weaker function of molar mass in the considered block copolymers, presumably a result of both the decreased free volume contribution from chain ends as well as differences in solvent partitioning in block copolymers compared to homopolymer solutions.

3.4.2 Ordering Quality

3.4.2.1 Concentrated Solution

Increased degree of oligomerization in the protein block of rcSso7d.SA oligomer-PNIPAM conjugates produces a significantly enhanced ordering quality in concentrated solution. This improved ordering is apparent by mere visual inspection of the SAXS curves for each conjugate at the concentration where the strongest ordering is observed at 25 °C (**Figure 3-4a**). While 1xSP9.8k shows a single, broad scattering peak indicative of disordered structure, all three

conjugates containing oligomerized rcSso7d.SA protein blocks display long-range periodic structures, as signified by the presence of higher-order scattering peaks. As the degree of oligomerization of the protein block increases, scattering peaks narrow, and ordering quality improves.

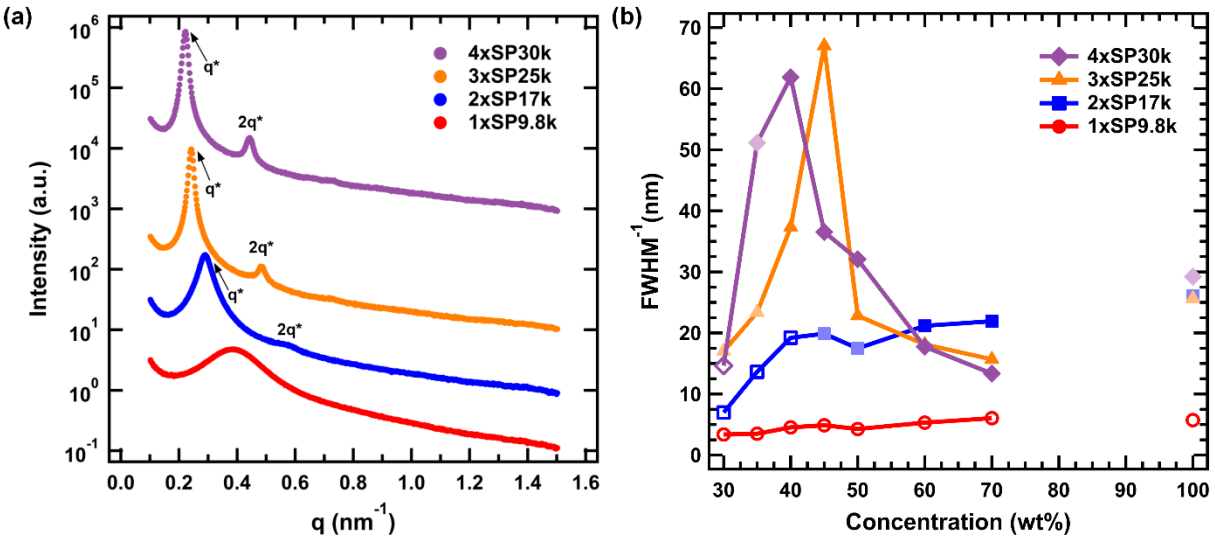

Figure 3-4. Ordering quality of rcSso7d.SA oligomer-PNIPAM conjugates indicated through (a) SAXS curves and (b) FWHM^{-1} of the primary scattering peak, where greater FWHM^{-1} values correspond to stronger ordering. SAXS curves in (a) are each collected at 25 °C, with the curves for 1xSP9.8k, 2xSP17k, and 3xSP25k collected at 45 wt. % and the curve for 4xSP30k collected at 40 wt. %. In graph (b), open symbols represent disordered phases, light symbols represent non-birefringent lamellar phases, and shaded symbols indicate a birefringent lamellar phase. Bulk data are disconnected from concentrated solution data to indicate that the 100 wt. % data are not at equilibrium.

A more quantitative measure of this enriched ordering can be obtained by calculating the full width at half maximum (FWHM) of the primary scattering peak. FWHM were calculated by simultaneously fitting a Lorentzian to the primary scattering peak and a background function to the scattering intensity as follows:

$$I(q) = \{Aq^{-4} + Bq^{-2} + C\} + \left\{I_0\left[\frac{\gamma^2}{(q-q_0)^2+\gamma^2}\right]\right\}, \qquad (3\text{-}1)$$

where the first term in braces accounts for background scattering with individual parameters to capture the scattering in the Porod regime, in the Guinier regime, and from a constant background,

and the second term in braces represent the Lorentzian fit where I_0 is the peak height, q_0 is the peak position, and 2γ is the FWHM. In **Figure 3-4b**, where $FWHM^{-1}$ values are plotted so greater values correspond to stronger ordering, oligomerization of rcSso7d.SA can be seen to result in significantly larger $FWHM^{-1}$ values. Again, ordering increases with degree of oligomerization of the protein block, with 3xSP25k and 4xSP30k conjugates displaying highly-ordered structures between 40 and 45 wt. %. At concentrations less than 60 wt. %, the $FWHM^{-1}$ value also serves as a very good indicator of phase behavior in these four studied conjugates. For $FWHM^{-1}$ less than 18 nm, conjugates almost exclusively form disordered phases, for $FWHM^{-1}$ between 18 and 23 nm, primarily non-birefringent lamellae are observed, and for $FWHM^{-1}$ greater than 23 nm, conjugates self-assemble into birefringent lamellae. At and above 60 wt. %, however, these phase predictions fail, as all lamellae not in the bulk state are birefringent. This is expected based on previous studies where the materials are shown to transition into a nematic phase as concentration increases out of the lamellar region.[25]

3.4.2.2 Highly Concentrated Solution

Phase behavior in highly concentrated solutions (classified here as concentrations greater than or equal to 60 wt. %) deviates significantly from that at lower concentrations. At and above 60 wt. %, 3xSP25k and 4xSP30k conjugates experience a drop in $FWHM^{-1}$ from lower concentrations, suggesting a disordering of lamellar nanophases (**Figure 3-4b**). This observation is in stark contrast to typical phase behavior in concentrated block copolymer solutions, where ordering is predicted[26] and observed[50-51] to strictly increase as a function of concentration, regardless of solvent selectivity. Though uncommon, this type of disordering has previously been observed in block copolymer solutions, typically as re-entrant ODT phase behavior. In polystyrene-*b*-polyisoprene (PS-PI) diblock copolymers in diethyl phthalate, a strongly selective solvent for PS,

a thermotropic re-entrant ODT has been observed at low polymer concentration (ϕ = 0.2), where heating causes phase changes from a disordered micellar phase to FCC-arranged micelles and finally to a disordered phase.[52] A lyotropic re-entrant ODT has also been documented in PS-PI solutions in decane (selective for PI) between 10 and 16 wt. % as a BCC phase composed of PS-PI micelles disorders then re-forms the BCC phase.[53] In this latter system, the odd phase behavior has been postulated to be a non-equilibrium effect that results from kinetic trapping of the micelles as the cores become glassy.[51] Re-entrant ODT behavior has been observed in previously-studied protein-polymer conjugates at high concentration as well,[24-25] for which it has been hypothesized that protein-polymer interactions become net attractive at high concentration.[25]

In this study, domain spacing analysis also reveals atypical behavior for block copolymers in highly concentrated solutions. For diblock copolymer solutions, domain spacing analysis can be performed to reveal the selectivity of a solvent towards each block through a power law relationship: domain spacing d scales with polymer volume fraction ϕ according to $d \sim \phi^{-\beta}$, where the value of exponent β is indicative of solvent selectivity.[54] In general for nonselective and weakly selective solvents, β is negative, and domain spacing increases with polymer volume fraction as the solvent slightly preferentially migrates to the interfaces between phases to screen unfavorable interactions between the two blocks.[54-55] Conversely, for strongly selective solvents β becomes positive—as high as unity—as one phase swells with added solvent to minimize interfacial area and therefore unfavorable solvent interactions with the insoluble block. Previously, water has been found to be slightly selective for the PNIPAM block in protein-PNIPAM conjugates,[23] and—accordingly—lamellar domain spacing increases with concentration at relatively low concentrations in the rcSSo7d.SA oligomer conjugates considered here (**Figure 3-5a**). However, in highly concentrated solution, the domain spacing of all lamellae-forming conjugates decreases

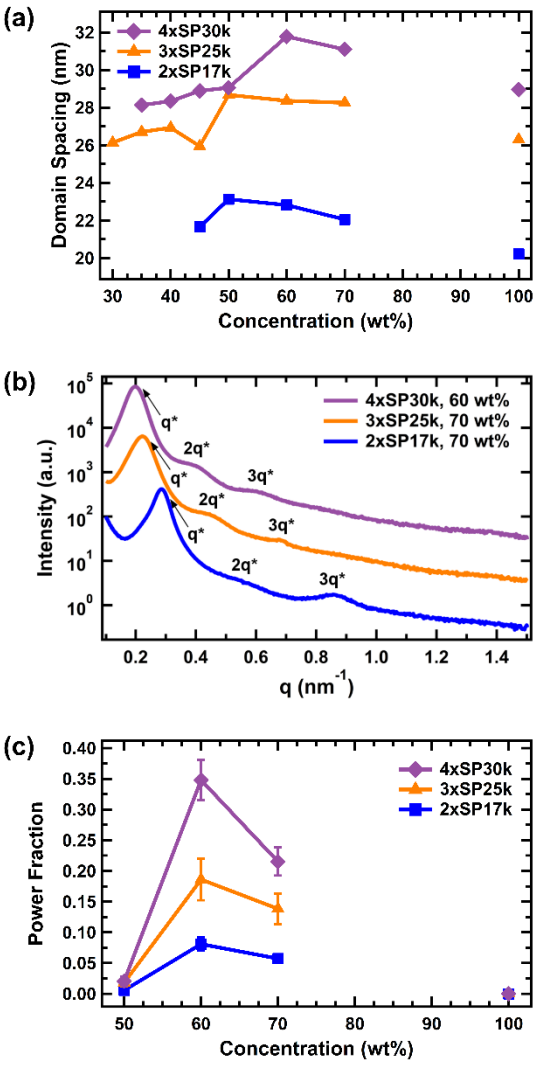

Figure 3-5. (a) Domain spacings in lamellar phases, (b) high concentration SAXS traces, and (c) average power fraction across heating and cooling cycles for 2xSP17k, 3xSP25k, and 4xSP30. Data in (a) and (b) are collected at 25 °C, and bulk data are disconnected from concentrated solution data to indicate that the 100 wt. % data are not at equilibrium. In (b) the low intensity of the $2q^*$ peak in the 2xSP17k scattering pattern is likely a result of a coincidence with a minimum in the form factor. Error bars in (c) represent standard deviation of the data set.

with increasing concentration, seemingly suggesting that water becomes a selective solvent at high concentration.

Similar domain spacing behavior has previously been observed in highly concentrated PS-PI solutions in toluene (a nonselective solvent) near room temperature,[56-57] for which it was proposed that the decrease in domain spacing resulted primarily from chain swelling effects due to reduced mobility of the polymer chains under these conditions. When incubated at room temperature, the conjugates in this study do in fact show a slight improvement in ordering as incubation time is increased (**Figure B-11**). While the results here display qualitative agreement with this theory, the PS-PI systems exhibited a continuous change in domain spacing across all compositions whereas the rcSso7d.SA oligomer-PNIPAM conjugates all contain a discontinuity between the regions of increasing and decreasing domain spacing. Thus, even if similar kinetic control of domain spacing is occurring in the studied systems, additional features of the

conjugates beyond chain swelling appear to also have a significant effect on the self-assembly dynamics, such as the hydrophobic interaction between PNIPAM and protein.[58-60] At high concentrations, these hydrophobic interactions may become relevant, resulting in an attractive force between PNIPAM and protein blocks that decreases domain spacing and disorders lamellar phases.

The long-range ordering of highly concentrated solutions of the studied bioconjugates exhibits key differences from that at lower concentrations. All lamellae-forming conjugates display q* reflections up to 3q* at concentrations at and above 60 wt. % (**Figure 3-5b**) while only reflections up to 2q* are observed at lower concentrations, indicating retention of lamellar ordering over longer length scales at higher concentration—at least within small grains. Birefringence signals also display substantial increases between 50 wt. % and 60 wt. % in these conjugates (**Figure 3-5c**). It is unlikely that these jumps in birefringence correspond to an improvement in long-range lamellar ordering, however, as 2xSP17k and 3xSP25k bulk samples also display lamellar reflections up to 3q* (**Figures B-3 to B-4**) but are not birefringent (**Figure 3-5c**). Indeed, even the 1xSP9.8k conjugates display a weak birefringent signal at 60 wt. % (**Table 3-2**, **Figure B-6f**) despite being highly disordered at this concentration. Instead, the increased birefringence signal is presumably a result of orientational ordering within the sample, similar to the nematic ordering previously observed at 70 and 80 wt. % in mCherry protein-polymer conjugates.[25]

3.4.3 Biosensing Capabilities

To confirm the sensing capabilities of rcSso7d.SA in oligomerized states, binding assays were performed. It has previously been demonstrated that protein-polymer block copolymers display size-exclusion properties in which molecular diffusion into the conjugates is controlled by diffusion through the polymer nanodomains, as only molecules of sufficiently lower molecular

weight than the polymer block can diffuse into the matrix.[31] Correspondingly, diffusion experiments using streptavidin—the biomolecule which rcSso7d.SA was genetically modified to bind—as the analyte displayed weak binding strength relative to an rcSso7d.SA monolayer (**Figure B-12**). It was reasoned that due to the large molar mass of streptavidin (53 kDa), very large (~100 kDa) PNIPAM molecules would need to be synthesized and conjugated to the rcSSo7d.SA oligomers to permit free diffusion. With a much higher polymer weight fraction, conjugates of these high-M_n PNIPAM molecules would represent a significant departure in ordering behavior from the symmetric weight fraction conjugates studied here. Because streptavidin is a tetrameric species, it was assumed that a smaller, monomeric streptavidin variant (14 kDa) would display only a slightly weaker binding strength to rcSso7d.SA due to the lack of multivalent binding effects[61-62] but experience little resistance to diffusion even in low molecular weight PNIPAM blocks. Thus, a monomeric form of streptavidin, mSA2,[63] was selected as the analyte for assays.

Binding assays were performed by adding serially diluted solutions of fluorescently-labeled mSA2 to thin films of each studied conjugate (**Figure 3-6a**). To maintain consistent transport properties between samples, each oligomer was conjugated to the same previously-synthesized 25 kDa PNIPAM sample. Analyte bound to thin films was quantified using fluorescence microscopy, and binding curves were fit to the collected mean fluorescent intensity (MFI) data using the following equation:

$$\mathrm{MFI} = \frac{\alpha}{2}\left(\beta - \sqrt{\beta^2 - 4\gamma}\right), \tag{3-2}$$

where α is the average MFI per binding event, β represents the sum of the total concentration of analyte molecules, total concentration of binding sites, and dissociation constant describing the

binding equilibrium, and γ is the product of two aforementioned concentrations. A derivation of this equation is provided in **Chapter 2**.

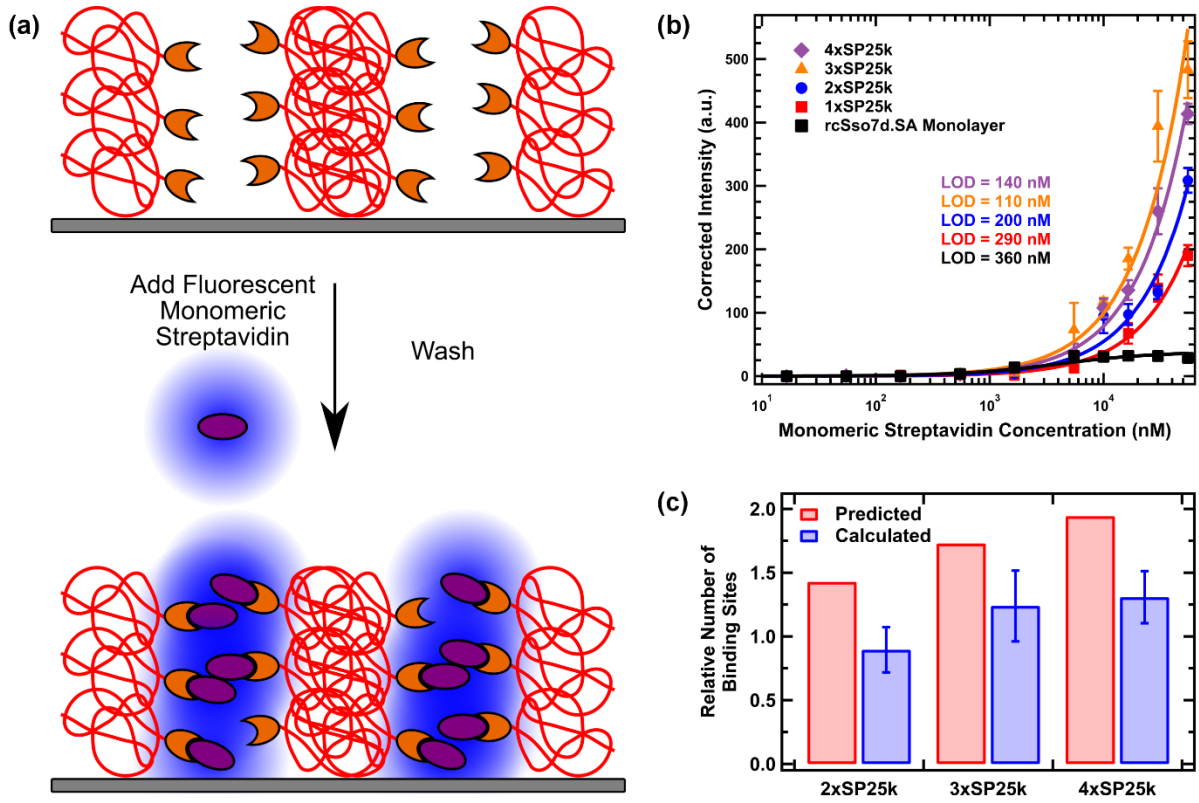

Figure 3-6. (a) Schematic representation of fluorescent binding assays performed within rcSso7d.SA oligomer-PNIPAM conjugate thin films. (b) Comparison of binding curves obtained for each considered conjugate and rcSso7d.SA monolayer. All curves are shifted to a background signal of 0 for clarity. Thicknesses for the 1xSP9.8k, 2xSP17k, 3xSP25k, and 4xSP30k films are 155, 130, 150, and 170 nm, respectively. Error bars represent the standard deviation of three replicates. (c) Predicted and calculated relative number of binding sites in each conjugate thin film. All values are relative to the number of binding sites in the 1xSP9.8k thin film. Error bars represent 95% confidence intervals for the calculated relative number of binding sites.

Curve fits performed on the binding assay data gave reasonable parameter values. Each fit yielded the same α value—which should be independent of sensor type—within the parameter uncertainty, demonstrating good self-consistency of the model. All thin film sensors also gave values for the total concentration of accessible binding sites $[P]_T$ significantly greater than that for the monolayer, as expected due to the greater thickness and thus total protein present in the thin films. Dissociation constant K_d values for the conjugate thin film biosensors, however, are

unreasonably large. These extremely high values likely result from the apparent rightward shift in fluorescent intensity values compared to the monolayer; since the K_d parameter is the only parameter in the used model that can significantly control left/right movement of the binding curve, this value presumably increased to accommodate the shift. As such, the K_d values reported for the thin film biosensors should be interpreted as fitting parameters only, as the values are not physically reasonable. Though it leads to inflated K_d values, the rightward shift of the binding curve in the thin film samples is consistent with behavior previously observed when increasing the concentration of binding sites within a protein biosensor.[18]

Table 3-3. Best-fit Parameter Values for Fits to Monomeric Streptavidin Binding Assays

Biosensor	α^a (MFI)	$[P]_T{}^a$ (nM)	$K_d{}^a$ (nM)
rcSso7d.SA Monolayer	100 ± 10	0.34 ± 0.05	2000 ± 1000
1xSP25k Thin Film	100 ± 10	3100 ± 400	$8\times10^7 \pm 1\times10^7$
2xSP25k Thin Film	100 ± 10	3300 ± 500	$6.0\times10^7 \pm 9\times10^6$
3xSP25k Thin Film	120 ± 20	3900 ± 700	$4.7\times10^7 \pm 9\times10^6$
4xSP25k Thin Film	112 ± 9	3700 ± 300	$5.2\times10^7 \pm 4\times10^6$

[a]Reported errors represent 95% confidence intervals for the parameter estimate.

Analysis of binding curves indicates that rcSso7d.SA oligomer conjugates not only retain binding capacity, but also significantly enhance rcSso7d.SA biosensing capabilities (**Figure 3-6b**). All conjugate samples show increased fluorescent signal at high concentration relative to a rcSso7d.SA monolayer, with the conjugate of the trimer displaying an improvement of over an order of magnitude at the highest measured concentration. Additionally, while the fluorescent intensity of the monolayer saturates for concentrations above 5 µM, all thin film samples show continually increasing signal at high analyte concentrations. Unlike the monolayer, the thin film samples contain densely-packed proteins in three-dimensions, thereby providing substantially more binding sites within the sensor and allowing distinction between a greater range of analyte concentrations before saturating. All binding curves are also considerably right-shifted compared to previously-reported curves for rcSso7d.SA in yeast-display experiments (K_d ~ 500 pM),[39]

though the presence of an equivalent shift in the monolayer binding curve indicates that the weaker binding is not a result of inherently worse binding kinetics within the conjugate thin films. The monolayer curve does, however, indicate similar binding strength compared to previous surface-immobilized rcSso7d.SA assays using streptavidin as the analyte,[18, 39] indicating that rcSso7d.SA has similar binding affinities for streptavidin and mSA2.

Oligomerization of rcSso7d.SA also brings about a decrease in biosensor limit of detection (LOD). By calculating LOD using the standard definition as the minimum concentration which gives a signal three standard deviations above that of the average blank, it is found that the LODs for the monolayer and 1xSP25k, 2xSP25k, 3xSP25k, and 4xSP25k thin films are 360, 290, 200, 110, and 140 nM, respectively. While all thin films display improvements up to threefold in LOD over the monolayer, the trend in LOD with respect to degree of oligomerization is non-monotonic. The primary factor that is expected to affect LOD in the studied biosensors is number of binding sites, as more binding sites enable a greater number of analyte molecules to be captured and shifts analyte-receptor equilibrium in favor of binding events. Since the number of binding sites is a function of both the density of accessible rcSso7d.SA proteins within a plane parallel to the underlying substrate and the number of these planes within a biosensor, both rcSso7d.SA volume fraction and film thickness are required to determine the number of these sites.

Calculation of the number of binding sites reveals a significant increase in both number and density of available sites in conjugate thin films relative to rcSso7d.SA monolayers. To determine the density of binding proteins within a single plane of each thin film, the concentration of accessible binding sites throughout the entire film—taken directly from the binding assay curve fits (**Table 3-3**)—was multiplied by the corresponding film thickness. When accounting for differences in film thickness, the density of oligomerized rcSso7d.SA proteins capable of binding

mSA2 is found to increase monotonically with degree of oligomerization (**Table B-1**). This calculated density decreases, though, between the 1xSP25k and 2xSP25k thin films, indicating a lower density of accessible binding sites in the protein domains of the oligomerized rcSso7d.SA conjugate film. The total number of predicted binding sites within each thin film assuming complete accessibility should be proportional to the volume fraction of rcSso7d.SA in the conjugate with PNIPAM. Reasonable estimates for relative values of the predicted number of sites can thus be obtained by normalizing the weight fraction of rcSso7d.SA in each conjugate by the corresponding weight fraction in 1xSP25k. Comparing these predicted relative number of binding sites to the calculated values (**Figure 3-6c**), all oligomeric rcSso7d.SA conjugates are found to contain fewer proteins capable of binding mSA2 than predicted. It is likely that this effect results from a combination of steric blocking of binding sites by bound mSA2 molecules as well as an absence of the free volume required to incorporate mSA2 molecules into the protein nanodomains at high degrees of binding. Despite the lower than expected binding capacity of the conjugate thin films, these biosensors contain approximately 10^4 times the quantity of accessible binding sites compared to rcSso7d.SA monolayers on a volumetric basis (**Table 3-3**). Recognizing that each plane (and a monolayer) of rcSso7d.SA proteins is roughly 1-2 nm thick,[64] the studied thin films can be determined to contain approximately 100 more planes of protein than a monolayer. Therefore, by accounting for differences in height between the thin films and monolayers, the thin films are found to contain around 2 orders of magnitude more moles of accessible protein per area, offering a significant improvement in protein density over traditional surface-immobilized protein biosensors.

3.5 Conclusions

The oligomerization of the low molecular weight protein rcSso7d.SA in protein-polymer conjugates is demonstrated to significantly improve the concentrated solution self-assembly in these materials. Block copolymers containing oligomerized rcSso7d.SA connected with flexible peptide sequences as a protein block display long-range lamellar ordering that is strongest in trimer and tetramer conjugates. In highly concentrated solution, the studied conjugates assemble into weakly-ordered lamellae and display domain spacings that vary non-monotonically across the studied concentration range.

Thin films of the rcSso7d.SA oligomer conjugates are also found to function as highly sensitive biosensors, retaining binding capabilities and providing up to threefold decreases in limit of detection compared to traditionally-used protein monolayers. In general, oligomerization is observed to lower the limit of detection by increasing density of binding sites, but some evidence suggests too high protein densities result in inaccessibility of some sites. Despite not containing fully-accessible binding sites, the protein-polymer conjugate thin film biosensors are estimated to contain a 100-fold greater density of accessible sites within a single plane of conjugates than an rcSso7d.SA monolayer. By identifying a strategy that both improves ordering in low molecular weight protein-polymer conjugates and enables the development of more sensitive biosensors, this work provides a substantial framework for future research in protein design for both fundamental understanding of protein-polymer conjugate self-assembly and biosensing applications.

3.6 References

1. Bahadır, E. B.; Sezgintürk, M. K., Lateral flow assays: Principles, designs and labels. *TrAC, Trends Anal. Chem.* **2016,** *82*, 286-306, DOI: 10.1016/j.trac.2016.06.006
2. Li, J.; Macdonald, J., Multiplexed lateral flow biosensors: Technological advances for radically improving point-of-care diagnoses. *Biosens. Bioelectron.* **2016,** *83*, 177-192, DOI: 10.1016/j.bios.2016.04.021

3. Quesada-González, D.; Merkoçi, A., Nanoparticle-based lateral flow biosensors. *Biosens. Bioelectron.* **2015,** *73*, 47-63, DOI: 10.1016/j.bios.2015.05.050
4. Sajid, M.; Kawde, A.-N.; Daud, M., Designs, formats and applications of lateral flow assay: A literature review. *J. Saudi Chem. Soc.* **2015,** *19* (6), 689-705, DOI: 10.1016/j.jscs.2014.09.001
5. Yetisen, A. K.; Akram, M. S.; Lowe, C. R., Paper-based microfluidic point-of-care diagnostic devices. *Lab Chip* **2013,** *13* (12), 2210-2251, DOI: 10.1039/C3LC50169H
6. Yang, H.; Gijs, M. A. M., Micro-optics for microfluidic analytical applications. *Chem. Soc. Rev.* **2018,** *47* (4), 1391-1458, DOI: 10.1039/C5CS00649J
7. Myers, F. B.; Lee, L. P., Innovations in optical microfluidic technologies for point-of-care diagnostics. *Lab Chip* **2008,** *8* (12), 2015-2031, DOI: 10.1039/B812343H
8. Kim, D.; Herr, A. E., Protein immobilization techniques for microfluidic assays. *Biomicrofluidics* **2013,** *7* (4), 041501, DOI: 10.1063/1.4816934
9. Ling, M. M.; Ricks, C.; Lea, P., Multiplexing molecular diagnostics and immunoassays using emerging microarray technologies. *Expert Rev. Mol. Diagn.* **2007,** *7* (1), 87-98, DOI: 10.1586/14737159.7.1.87
10. Chandra, P. E.; Sokolove, J.; Hipp, B. G.; Lindstrom, T. M.; Elder, J. T.; Reveille, J. D.; Eberl, H.; Klause, U.; Robinson, W. H., Novel multiplex technology for diagnostic characterization of rheumatoid arthritis. *Arthrit. Res. Ther.* **2011,** *13* (3), R102, DOI: 10.1186/ar3383
11. Cracknell, J. A.; Vincent, K. A.; Armstrong, F. A., Enzymes as Working or Inspirational Electrocatalysts for Fuel Cells and Electrolysis. *Chem. Rev.* **2008,** *108* (7), 2439-2461, DOI: 10.1021/cr0680639
12. Makaraviciute, A.; Ramanaviciene, A., Site-directed antibody immobilization techniques for immunosensors. *Biosens. Bioelectron.* **2013,** *50* (Supplement C), 460-471, DOI: 10.1016/j.bios.2013.06.060
13. Squires, T. M.; Messinger, R. J.; Manalis, S. R., Making it stick: convection, reaction and diffusion in surface-based biosensors. *Nat. Biotechnol.* **2008,** *26* (4), 417-426, DOI: 10.1038/nbt1388
14. Ho, J.-a. A.; Hsu, W.-L.; Liao, W.-C.; Chiu, J.-K.; Chen, M.-L.; Chang, H.-C.; Li, C.-C., Ultrasensitive electrochemical detection of biotin using electrically addressable site-oriented antibody immobilization approach via aminophenyl boronic acid. *Biosens. Bioelectron.* **2010,** *26* (3), 1021-1027, DOI: 10.1016/j.bios.2010.08.048
15. Peluso, P.; Wilson, D. S.; Do, D.; Tran, H.; Venkatasubbaiah, M.; Quincy, D.; Heidecker, B.; Poindexter, K.; Tolani, N.; Phelan, M.; Witte, K.; Jung, L. S.; Wagner, P.; Nock, S., Optimizing antibody immobilization strategies for the construction of protein microarrays. *Anal. Biochem.* **2003,** *312* (2), 113-124, DOI: 10.1016/S0003-2697(02)00442-6
16. Boozer, C.; Ladd, J.; Chen, S.; Jiang, S., DNA-Directed Protein Immobilization for Simultaneous Detection of Multiple Analytes by Surface Plasmon Resonance Biosensor. *Anal. Chem.* **2006,** *78* (5), 1515-1519, DOI: 10.1021/ac051923l
17. Naal, Z.; Park, J. H.; Bernhard, S.; Shapleigh, J. P.; Batt, C. A.; Abruña, H. D., Amperometric TNT Biosensor Based on the Oriented Immobilization of a Nitroreductase Maltose Binding Protein Fusion. *Anal. Chem.* **2002,** *74* (1), 140-148, DOI: 10.1021/ac010596o
18. Miller, E. A.; Baniya, S.; Osorio, D.; Al Maalouf, Y. J.; Sikes, H. D., Paper-based diagnostics in the antigen-depletion regime: High-density immobilization of rcSso7d-cellulose-

binding domain fusion proteins for efficient target capture. *Biosens. Bioelectron.* **2018,** *102*, 456-463, DOI: 10.1016/j.bios.2017.11.050
19. Sinem, E.; Dagmar, F.; Doris, W.; Ljiljana, F., SNAP-tag as a Tool for Surface Immobilization. *Curr. Pharm. Des.* **2013,** *19* (30), 5443-5448, DOI: 10.2174/1381612811319300015
20. Wasserberg, D.; Cabanas-Danés, J.; Prangsma, J.; O'Mahony, S.; Cazade, P.-A.; Tromp, E.; Blum, C.; Thompson, D.; Huskens, J.; Subramaniam, V.; Jonkheijm, P., Controlling Protein Surface Orientation by Strategic Placement of Oligo-Histidine Tags. *ACS Nano* **2017,** *11* (9), 9068-9083, DOI: 10.1021/acsnano.7b03717
21. Thomas, C. S.; Glassman, M. J.; Olsen, B. D., Solid-State Nanostructured Materials from Self-Assembly of a Globular Protein–Polymer Diblock Copolymer. *ACS Nano* **2011,** *5* (7), 5697-5707, DOI: 10.1021/nn2013673
22. Thomas, C. S.; Xu, L.; Olsen, B. D., Kinetically Controlled Nanostructure Formation in Self-Assembled Globular Protein–Polymer Diblock Copolymers. *Biomacromolecules* **2012,** *13* (9), 2781-2792, DOI: 10.1021/bm300763x
23. Lam, C. N.; Olsen, B. D., Phase transitions in concentrated solution self-assembly of globular protein-polymer block copolymers. *Soft Matter* **2013,** *9* (8), 2393-2402, DOI: 10.1039/C2SM27459K
24. Thomas, C. S.; Olsen, B. D., Coil fraction-dependent phase behaviour of a model globular protein-polymer diblock copolymer. *Soft Matter* **2014,** *10* (17), 3093-3102, DOI: 10.1039/C3SM52531G
25. Chang, D.; Lam, C. N.; Tang, S.; Olsen, B. D., Effect of polymer chemistry on globular protein-polymer block copolymer self-assembly. *Polymer Chemistry* **2014,** *5* (17), 4884-4895, DOI: 10.1039/C4PY00448E
26. Huang, C.-I.; Lodge, T. P., Self-Consistent Calculations of Block Copolymer Solution Phase Behavior. *Macromolecules* **1998,** *31* (11), 3556-3565, DOI: 10.1021/ma980007p
27. Qin, G.; Glassman, M. J.; Lam, C. N.; Chang, D.; Schaible, E.; Hexemer, A.; Olsen, B. D., Topological Effects on Globular Protein-ELP Fusion Block Copolymer Self-Assembly. *Adv. Funct. Mater.* **2015,** *25* (5), 729-738, DOI: 10.1002/adfm.201403453
28. Lam, C. N.; Kim, M.; Thomas, C. S.; Chang, D.; Sanoja, G. E.; Okwara, C. U.; Olsen, B. D., The Nature of Protein Interactions Governing Globular Protein–Polymer Block Copolymer Self-Assembly. *Biomacromolecules* **2014,** *15* (4), 1248-1258, DOI: 10.1021/bm401817p
29. Lam, C. N.; Yao, H.; Olsen, B. D., The Effect of Protein Electrostatic Interactions on Globular Protein–Polymer Block Copolymer Self-Assembly. *Biomacromolecules* **2016,** *17* (9), 2820-2829, DOI: 10.1021/acs.biomac.6b00522
30. Huang, A.; Qin, G.; Olsen, B. D., Highly Active Biocatalytic Coatings from Protein–Polymer Diblock Copolymers. *ACS Appl. Mater. Interfaces* **2015,** *7* (27), 14660-14669, DOI: 10.1021/acsami.5b01884
31. Dong, X. H.; Obermeyer, A. C.; Olsen, B. D., Three-Dimensional Ordered Antibody Arrays Through Self-Assembly of Antibody–Polymer Conjugates. *Angew. Chem. Int. Ed.* **2017,** *56* (5), 1273-1277, DOI: 10.1002/anie.201607085
32. Hassanzadeh-Ghassabeh, G.; Devoogdt, N.; Pauw, P. D.; Vincke, C.; Muyldermans, S., Nanobodies and their potential applications. *Nanomedicine* **2013,** *8* (6), 1013-1026, DOI: 10.2217/nnm.13.86
33. Wang, H.; Li, G.; Zhang, Y.; Zhu, M.; Ma, H.; Du, B.; Wei, Q.; Wan, Y., Nanobody-Based Electrochemical Immunoassay for Ultrasensitive Determination of Apolipoprotein-A1

Using Silver Nanoparticles Loaded Nanohydroxyapatite as Label. *Anal. Chem.* **2015,** *87* (22), 11209-11214, DOI: 10.1021/acs.analchem.5b04063
34. Li, H.; Sun, Y.; Elseviers, J.; Muyldermans, S.; Liu, S.; Wan, Y., A nanobody-based electrochemiluminescent immunosensor for sensitive detection of human procalcitonin. *Analyst* **2014,** *139* (15), 3718-3721, DOI: 10.1039/C4AN00626G
35. Renberg, B.; Nordin, J.; Merca, A.; Uhlén, M.; Feldwisch, J.; Nygren, P.-Å.; Eriksson Karlström, A., Affibody Molecules in Protein Capture Microarrays: Evaluation of Multidomain Ligands and Different Detection Formats. *J. Proteome Res.* **2007,** *6* (1), 171-179, DOI: 10.1021/pr060316r
36. Nygren, P. Å., Alternative binding proteins: Affibody binding proteins developed from a small three-helix bundle scaffold. *FEBS J.* **2008,** *275* (11), 2668-2676, DOI: 10.1111/j.1742-4658.2008.06438.x
37. Miranda, F. F.; Brient-Litzler, E.; Zidane, N.; Pecorari, F.; Bedouelle, H., Reagentless fluorescent biosensors from artificial families of antigen binding proteins. *Biosens. Bioelectron.* **2011,** *26* (10), 4184-4190, DOI: 10.1016/j.bios.2011.04.030
38. Traxlmayr, M. W.; Kiefer, J. D.; Srinivas, R. R.; Lobner, E.; Tisdale, A. W.; Mehta, N. K.; Yang, N. J.; Tidor, B.; Wittrup, K. D., Strong Enrichment of Aromatic Residues in Binding Sites from a Charge-neutralized Hyperthermostable Sso7d Scaffold Library. *J. Biol. Chem.* **2016,** *291* (43), 22496-22508, DOI: 10.1074/jbc.M116.741314
39. Miller, E. A.; Traxlmayr, M. W.; Shen, J.; Sikes, H. D., Activity-based assessment of an engineered hyperthermophilic protein as a capture agent in paper-based diagnostic tests. *Mol. Syst. Des. Eng.* **2016,** *1* (4), 377-381, DOI: 10.1039/C6ME00032K
40. Zhao, N.; Spencer, J.; Schmitt, M. A.; Fisk, J. D., Hyperthermostable binding molecules on phage: Assay components for point-of-care diagnostics for active tuberculosis infection. *Anal. Biochem.* **2017,** *521*, 59-71, DOI: 10.1016/j.ab.2016.12.021
41. Kalichuk, V.; Béhar, G.; Renodon-Cornière, A.; Danovski, G.; Obal, G.; Barbet, J.; Mouratou, B.; Pecorari, F., The archaeal "7 kDa DNA-binding" proteins: extended characterization of an old gifted family. *Sci. Rep.* **2016,** *6*, 37274, DOI: 10.1038/srep37274
42. Chang, D.; Huang, A.; Olsen, B. D., Kinetic Effects on Self-Assembly and Function of Protein–Polymer Bioconjugates in Thin Films Prepared by Flow Coating. *Macromol. Rapid Commun.* **2017,** *38* (1), 1600449, DOI: 10.1002/marc.201600449
43. Dixit, C. K.; Vashist, S. K.; MacCraith, B. D.; O'Kennedy, R., Multisubstrate-compatible ELISA procedures for rapid and high-sensitivity immunoassays. *Nat. Prot.* **2011,** *6*, 439, DOI: 10.1038/nprot.2011.304
44. Schneider, C. A.; Rasband, W. S.; Eliceiri, K. W., NIH Image to ImageJ: 25 years of image analysis. *Nat. Methods* **2012,** *9*, 671, DOI: 10.1038/nmeth.2089
45. Baumann, H.; Knapp, S.; Lundbäck, T.; Ladenstein, R.; Härd, T., Solution structure and DNA-binding properties of a thermostable protein from the archaeon Sulfolobus solfataricus. *Nat. Struct. Biol.* **1994,** *1*, 808, DOI: 10.1038/nsb1194-808
46. Chen, X.; Zaro, J. L.; Shen, W.-C., Fusion protein linkers: Property, design and functionality. *Adv. Drug Del. Rev.* **2013,** *65* (10), 1357-1369, DOI: 10.1016/j.addr.2012.09.039
47. Olsen, B. D.; Shah, M.; Ganesan, V.; Segalman, R. A., Universalization of the Phase Diagram for a Model Rod−Coil Diblock Copolymer. *Macromolecules* **2008,** *41* (18), 6809-6817, DOI: 10.1021/ma800978c

48. Xia, Y.; Yin, X.; Burke, N. A. D.; Stöver, H. D. H., Thermal Response of Narrow-Disperse Poly(N-isopropylacrylamide) Prepared by Atom Transfer Radical Polymerization. *Macromolecules* **2005,** *38* (14), 5937-5943, DOI: 10.1021/ma050261z
49. Lessard, D. G.; Ousalem, M.; Zhu, X. X., Effect of the molecular weight on the lower critical solution temperature of poly(N,N-diethylacrylamide) in aqueous solutions. *Can. J. Chem.* **2001,** *79* (12), 1870-1874, DOI: 10.1139/v01-180
50. Lodge, T. P.; Hanley, K. J.; Pudil, B.; Alahapperuma, V., Phase Behavior of Block Copolymers in a Neutral Solvent. *Macromolecules* **2003,** *36* (3), 816-822, DOI: 10.1021/ma0209601
51. Lodge, T. P.; Pudil, B.; Hanley, K. J., The Full Phase Behavior for Block Copolymers in Solvents of Varying Selectivity. *Macromolecules* **2002,** *35* (12), 4707-4717, DOI: 10.1021/ma0200975
52. Hanley, K. J.; Lodge, T. P.; Huang, C.-I., Phase Behavior of a Block Copolymer in Solvents of Varying Selectivity. *Macromolecules* **2000,** *33* (16), 5918-5931, DOI: 10.1021/ma000318b
53. McConnell, G. A.; Gast, A. P., Melting of Ordered Arrays and Shape Transitions in Highly Concentrated Diblock Copolymer Solutions. *Macromolecules* **1997,** *30* (3), 435-444, DOI: 10.1021/ma961241n
54. Lai, C.; Russel, W. B.; Register, R. A., Scaling of Domain Spacing in Concentrated Solutions of Block Copolymers in Selective Solvents. *Macromolecules* **2002,** *35* (10), 4044-4049, DOI: 10.1021/ma0122223
55. Lodge, T. P.; Hamersky, M. W.; Hanley, K. J.; Huang, C.-I., Solvent Distribution in Weakly-Ordered Block Copolymer Solutions. *Macromolecules* **1997,** *30* (20), 6139-6149, DOI: 10.1021/ma970720z
56. Shibayama, M.; Hashimoto, T.; Hasegawa, H.; Kawai, H., Ordered structure in block polymer solutions. 3. Concentration dependence of microdomains in nonselective solvents. *Macromolecules* **1983,** *16* (9), 1427-1433, DOI: 10.1021/ma00243a005
57. Hashimoto, T.; Shibayama, M.; Kawai, H., Ordered structure in block polymer solutions. 4. Scaling rules on size of fluctuations with block molecular weight, concentration, and temperature in segregation and homogeneous regimes. *Macromolecules* **1983,** *16* (7), 1093-1101, DOI: 10.1021/ma00241a010
58. Kawaguchi, H.; Fujimoto, K.; Mizuhara, Y., Hydrogel microspheres III. Temperature-dependent adsorption of proteins on poly-N-isopropylacrylamide hydrogel microspheres. *Colloid. Polym. Sci.* **1992,** *270* (1), 53-57, DOI: 10.1007/bf00656929
59. Gan, D.; Lyon, L. A., Synthesis and Protein Adsorption Resistance of PEG-Modified Poly(N-isopropylacrylamide) Core/Shell Microgels. *Macromolecules* **2002,** *35* (26), 9634-9639, DOI: 10.1021/ma021186k
60. Duracher, D.; Elaïssari, A.; Mallet, F.; Pichot, C., Adsorption of Modified HIV-1 Capsid p24 Protein onto Thermosensitive and Cationic Core−Shell Poly(styrene)−Poly(N-isopropylacrylamide) Particles. *Langmuir* **2000,** *16* (23), 9002-9008, DOI: 10.1021/la0004045
61. Dubacheva, G. V.; Araya-Callis, C.; Geert Volbeda, A.; Fairhead, M.; Codée, J.; Howarth, M.; Richter, R. P., Controlling Multivalent Binding through Surface Chemistry: Model Study on Streptavidin. *J. Am. Chem. Soc.* **2017,** *139* (11), 4157-4167, DOI: 10.1021/jacs.7b00540
62. Pérez-Luna, V. H.; O'Brien, M. J.; Opperman, K. A.; Hampton, P. D.; López, G. P.; Klumb, L. A.; Stayton, P. S., Molecular Recognition between Genetically Engineered

Streptavidin and Surface-Bound Biotin. *J. Am. Chem. Soc.* **1999,** *121* (27), 6469-6478, DOI: 10.1021/ja983984p
63. DeMonte, D.; Drake, E. J.; Lim, K. H.; Gulick, A. M.; Park, S., Structure-based engineering of streptavidin monomer with a reduced biotin dissociation rate. *Proteins: Struct., Funct., Bioinf.* **2013,** *81* (9), 1621-1633, DOI: 10.1002/prot.24320
64. Merlino, A.; Graziano, G.; Mazzarella, L., Structural and dynamic effects of α-Helix deletion in Sso7d: Implications for protein thermal stability. *Proteins: Struct., Funct., Bioinf.* **2004,** *57* (4), 692-701, DOI: 10.1002/prot.20270